ELSEVIER

NeuroImage

www.elsevier.com/locate/ynimg
NeuroImage 24 (2005) 82–91

An evaluation of the use of passive shimming to improve frontal sensitivity in fMRI

Rhodri Cusack,[a,*] Benedict Russell,[b] Sylvia M.L. Cox,[a,c] Claudia De Panfilis,[d] Christian Schwarzbauer,[a] and Richard Ansorge[b]

[a]*MRC Cognition and Brain Sciences Unit, Cambridge, UK*
[b]*Cavendish Physics Laboratories, University of Cambridge, UK*
[c]*Experimental Psychopharmacology Unit, Brain and Behaviour Institute, Universiteit Maastricht, The Netherlands*
[d]*Wolfson Brain Imaging Centre, University of Cambridge, UK*

Received 30 January 2004; revised 30 July 2004; accepted 23 August 2004
Available online 18 November 2004

The presence of the head in an MRI scanner leads to inhomogeneities in the magnetic field. These cause the 'susceptibility artifacts' of image distortion and signal dropout. In this paper, we evaluate a technique called passive shimming, which has the potential to reduce field inhomogeneities and the resultant artifacts. A piece of a magnetically active material (pyrolytic graphite) is held on the roof of the participant's mouth by a plastic mouth mould. We evaluate the effects in several different ways. We show that the presence of a shim reduces field inhomogeneity across much of the brain. From field maps, we generate simulations of EPI image intensity and BOLD sensitivity. Both of these are mainly improved by the presence of shim, although there were small reductions in some regions. Measured EPI image intensity also mostly increased. Finally, we ran a reward–punishment task in our subjects, and found that the presence of a shim increased functional sensitivity in the orbitofrontal cortex. Using the BOLD sensitivity measure, we provide estimates of the improvement to be expected in functional studies for a range of neural structures. Passive shims are quick to make and reasonably comfortable to wear, and have substantial potential for researchers investigating inferior frontal brain regions using MRI.

Keywords: Inhomogeneity; Brain; Reward–punishment task

Introduction

Ideally, the magnetic field throughout the bore of an MRI scanner would be homogeneous. Inhomogeneities in the field lead to two main problems in sequences such as the one most commonly used for functional imaging, gradient-echo echo planar imaging (EPI). First, images become distorted. Distortions can be effectively corrected by collecting maps of the magnetic field and then by applying post hoc corrections as discussed elsewhere (Cusack et al., 2003) and are not tackled here. A second problem is that signal is lost in the inferior frontal and anterior temporal regions, leading to low sensitivity to functional changes. The resulting black holes in EPI images are usually called 'dropout' or 'susceptibility artefact'. This paper primarily focuses on this second problem of signal dropout in the inferior frontal lobe.

While it is easy to design coils that give a fairly homogeneous field when the scanner is empty, as soon as a person is placed in the scanner, the different magnetic properties of air and tissue introduce inhomogeneities in the field. Some of these inhomogeneities can be removed by applying small corrective gradients using a set of coils designed for this purpose—a procedure referred to here as *active shimming* (but often just called shimming). However, these coils can only correct for relatively coarse, low spatial frequency inhomogeneities in the field, and substantial field inhomogeneities remain around the inferior temporal lobe caused by the tissue–air boundary at the mastoid sinuses, and around the inferior frontal lobe caused by the tissue–air boundaries in the mouth and frontal sinuses. This leads to the signal dropout in these regions.

In this paper, we evaluate a technique proposed by Wilson et al. (2002) in which a piece of material with particular magnetic properties is placed in the mouth while participants are being scanned. The idea is that the distortions introduced by the magnetic material cancel out some of the distortions due to the head and result in a more homogeneous field in the brain. This procedure is called *passive shimming* because the field corrections are achieved merely by the interaction of the magnetically active material with the static field, rather than the addition of any extra field using coils.

To evaluate the technique, we acquired maps of the magnetic field, and EPI data. The magnetic field maps were used to quantify the degree of field inhomogeneity (magnitude of field gradient, MFG), and to simulate the effects of field variations on the EPI

* Corresponding author. MRC Cognition and Brain Sciences Unit, 15 Chaucer Road, Cambridge, CB2 2EF, UK. Fax: +44 1223 359062.
E-mail address: rhodri.cusack@mrc-cbu.cam.ac.uk (R. Cusack).
Available online on ScienceDirect (www.sciencedirect.com.)

1053-8119/$ - see front matter © 2004 Elsevier Inc. All rights reserved.
doi:10.1016/j.neuroimage.2004.08.029

data. Two important characteristics of EPI data were examined: the EPI image intensity (II) and the BOLD sensitivity (BS). The EPI image intensity was simulated from the fieldmaps (sII) and measured directly from the EPI data (mII). The simulation used a model presented by Deichmann et al. (2002). The BOLD sensitivity was also simulated from the fieldmaps using this model (sBS). To empirically test for an increase in BOLD sensitivity, we conducted an fMRI experiment using a task that activates a region where passive shimming gives most improvement, in the orbitofrontal cortex (fMRI) (Wilson et al., 2003). This validation using fMRI is important, because there are factors limiting sensitivity in functional activation experiments that are not accounted for by Deichmann et al's (2002) model. For example, neither subject movement, nor the influence of physiological rather than measurement noise, are considered. The effect of these factors is considered further in Discussion.

The field map and EPI measurements were acquired twice in each subject. Within each session, they were taken while the subjects wore the passive shim, and again while they wore a dummy ("sham") shim that did not contain the magnetically active material. The use of a sham shim ensured that the differences in functional activation observed were not due to any distracting effect of the presence of the object in the mouth. In each subject, it was therefore possible to derive each of the measurements above (MFG, sII, mII, sBS, fMRI) while there were wearing the real and sham shims.

Method

General procedure

Ten participants were scanned in sessions lasting around 1.5–2 h. Ethical approval was obtained from the Cambridge Local Research Ethics Committee at Addenbrooke's NHS Trust. We used a Bruker Medspec 3 T system with a head gradient set. Two similar blocks were acquired in each session. In one, participants wore a passive shim comprising a plastic case containing an active magnetic material (construction described below). In the other block, participants wore a 'sham' shim that was just the plastic case. The order of acquisition of these two parts was counterbalanced across participants. At the start of each block, active shimming and coil tuning was done (i.e., twice in each participant).

In each block, we acquired maps of the magnetic field using a pair of gradient echo acquisitions, using the Bruker GEFI-TOMO protocol. The matrix size in the x (left–right), y (anterior–posterior), and z (inferior–superior) directions, respectively, was 64 × 256 × 64 and the resolution 4 × 1 × 4 mm. The two acquisitions were identical in all ways apart from their echo time, which was 7 ms in the first and 16.104 ms in the second. Complex reconstruction of each acquisition was performed. The magnitude of the first was used. A phase difference was calculated by subtracting the phase in the acquisition with the longer TE from the phase in the other. After phase unwrapping (Cusack and Papadakis, 2002), this phase difference is proportional to the magnetic field inhomogeneity according to the relationship:

$$\Delta B(r) = \frac{\Delta\Phi(r)}{\gamma \cdot \Delta TE}$$

where $\Delta B(r)$ is the field inhomogeneity at point r, $\Delta\Phi(r)$ is the phase difference at point r, ΔTE is the difference in echo times, γ is in units of radians/T/s (2.675×10^8).

The difference of 9.104 ms was used because it is a multiple of the precession time for fat versus water at 3 T, and so this component cancels out.

In each block, we acquired BOLD-EPI volumes while subjects performed a task described below. The data from 2 of the 10 subjects were discarded as they moved excessively. In four or the remaining subjects, we acquired 610 EPI volumes and in another four 620 EPI volumes, of 21 slices each with a matrix size of 64 × 64 with a slice thickness of 4 mm, inter-slice gap of 1 mm and an in-plane resolution of 3.125 × 3.125 mm. The TR was 1100 ms and TE 27.5 ms. The acquisition window was 40.6 ms in duration. The acquisition was symmetrical, so that in the absence of inhomogeneities, the center of k-space would have been in the middle of this window. The sign of the phase blips was such that the k-space trajectory started at positive k_y and ended at negative k_y.

Shim construction

We constructed the shims using a procedure supplied by James Wilson at fMRIB in Oxford, UK (see also Wilson et al., 2002). The magnetic material was generously supplied on a trial basis by Minteq International Inc, PA. It was pyrolytic graphite, which has highly anisotropic susceptibility. Perpendicular to the basal plane of the graphite, it is the most diamagnetic solid material known. The graphite was held by a plastic case moulded to the shape of the roof of the subjects mouth and held in place securely by the teeth in a similar way to a gumshield used for sports. A picture of the graphite and plastic case is shown in Fig. 1. Hygiene was ensured by using fresh plastic for each person, placed in boiling water before molding. The graphite was sealed

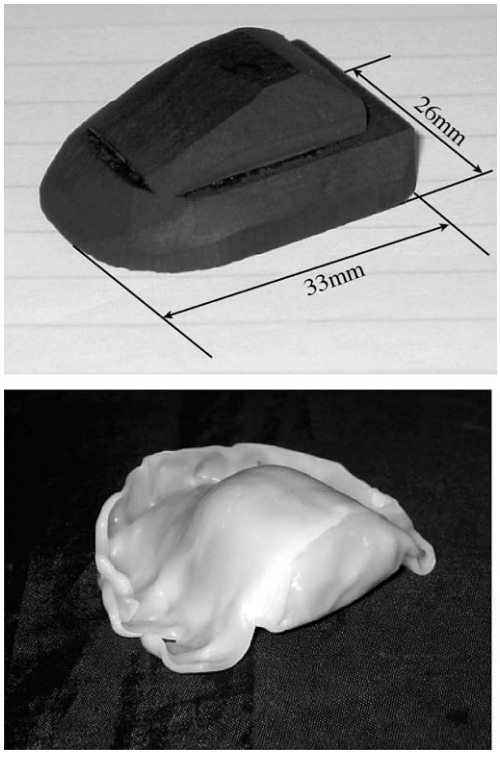

Fig. 1. The graphite shim (top) and plastic mouth mould that contained it (bottom).

in plastic, but in case of leakage, it was cleaned thoroughly before each use.

Analysis of field maps

Magnetic field measurements were obtained when the subjects were wearing the real and sham shims. Three summary measures were derived from each of these maps. Each gave a slightly different predictor of signal loss as a function of position.

Magnitude of field gradient (MFG)

This measure was the most simple and most direct. Signal loss is caused by gradients in the magnetic field strength, rather than the field strength itself. The simplest summary measure of the rate of change of the field is the magnitude of this gradient.

$$m = |\nabla B| = \sqrt{\left(\frac{\partial B}{\partial x}\right)^2 + \left(\frac{\partial B}{\partial y}\right)^2 + \left(\frac{\partial B}{\partial z}\right)^2}$$

where m = magnitude of gradient of field strength, B = z component of field strength.

Simulated EPI image intensity (sII)

This measure was derived using the equations from Diechmann et al. (2002). Their model accounts for the anisotropic effect of magnetic field gradients on EPI image intensity. In the slice encode (z) direction, the main effect of gradients is to cause within-voxel dephasing. Gradients in the phase (y) direction lead to several different effects, which can be best explained by considering the effect of the gradients on the actual trajectory obtained in k-space. They define a dimensionless variable Q, an effective echo time TE, and factor providing the amount of dephasing in the z direction F:

$$Q = 1 - \frac{\gamma \cdot \Delta t}{2\pi} \cdot FoV \cdot \frac{\partial B}{\partial y}$$

where Δt is the time taken to acquire a single line in k-space (6.4×10^{-4} s for a read (x) matrix size of 64 voxels and sample rate of 101 kHz), FoV is the field of view in the phase encode direction, $\partial B/\partial y$ is the gradient of the magnetic field in the phase encode (y) direction.

$$TE = \frac{TC}{Q}$$

where TE is the effective (i.e., achieved) echo time, TC is the central ("desired") echo time, which would be obtained in the absence of field gradients. Note that this is the value usually quoted as TE in papers.

$$F = \frac{\partial B}{\partial z} \cdot \frac{TE \cdot \gamma \cdot \Delta z}{4\sqrt{\ln 2}}$$

where $\partial B/\partial z$ is the gradient of the magnetic field in the slice-select (z) direction, Δz is the FWHM thickness of Gaussian slices in the z direction.

These factors can then be used to elegantly estimate the image intensity. First, if the k-space trajectory is so distorted that it does not reach the center of k-space, which contains most of the energy in the acquisition, then there will be complete signal loss.

If

$$\frac{\partial B}{\partial y} > \frac{2\pi(1 - \frac{TC}{t_{\text{start}}})}{\gamma \cdot \Delta t \cdot FoV} \text{ and } \frac{\partial B}{\partial y} < \frac{2\pi(1 - \frac{TC}{t_{\text{end}}})}{\gamma \cdot \Delta t \cdot FoV}$$

where t_{start},, t_{end} are the times after excitation when acquisition starts and ends

$$\text{then } sII(x,y,z) = \frac{1}{Q} \cdot e^{-F^2} \cdot \frac{e^{-\frac{TE}{T2*}}}{e^{-\frac{TC}{T2*}}}$$

otherwise $sII(x,y,z) = 0$

The three main terms in this final equation correspond to three different effects on image intensity. The initial $1/Q$ reflects the change in density of sampling in k-space in the phase encode direction, due to the additional gradient. The second term, the Gaussian-like exponential, reflects dephasing due to gradients in the z (slice-select) direction. And the third term reflects the actual amount of T2* decay due to the difference between the TE and TC. T2* was taken to be 40 ms. We included an additional normalization factor of $e^{-TC/T2*}$, so that without any field gradients, image intensity is unity.

Measured EPI image intensity (mII)

The image intensity was also directly measured in the EPI data. Informally, EPI image intensity is often used to assess dropout by eye, when researchers look for black holes in their images. We compared the simulated and measured image intensities, and also performed a statistical analysis across shim conditions.

Simulated BOLD sensitivity (sBS)

This measure is derived from sII, but with an additional factor due to the effect of the change in effective echo time on BOLD sensitivity (sBS = sII*TE/TC). The longer the echo time, the larger the effect of the small gradients that lead to the BOLD effect. However, T2* decay is greater and this causes signal loss. These two factors trade off against each other, and there is an optimum echo time determined by their balance (actually when TE = T2*). A shift of the effective echo time away from this reduces signal.

Statistical analysis: whole brain and ROI

For each of the four measures above (MFG, sII, sBS, mII), we calculated mean across subjects with the real and sham shims. SPM 99 (www.fil.ion.ucl.ac.uk/spm) was also used to compare the magnitude of the gradients between the real and sham shims across the whole brain. This was done in a similar way to that used to perform a second-level functional random-effects analysis. A paired t test was used to examine the effect of the shim across subjects. The false discovery rate (FDR) correction for multiple comparisons was used (Genovese et al., 2002).

To provide a summary measure of where in the brain BOLD sensitivity should be most affected, a region-of-interest analysis

was also performed. We used the Automated Anatomical Labeling (AAL) template (Tzourio-Mazoyer et al., 2002) to define a set of regions of interest. The improvement in each of these regions was then calculated using custom-written MATLAB code.

Functional imaging experiment (fMRI)

Background

Previous work has suggested that passive shimming substantially increases image intensity (Wilson et al., 2002, 2003) and signal stability during movement (Wilson and Jezzard, 2003) in inferior frontal regions. However, it has not actually been evaluated using an fMRI experiment. We conducted a reward–punishment task to assess functional activation in the orbitofrontal cortex (OFC). The OFC has been implicated in the representation of rewarding properties of stimuli or events (Elliott et al., 2003; Gottfried et al., 2002; Knutson et al., 2001; O'Doherty et al., 2001, 2002; Small et al., 2001), and in guiding responses in the context of rewarding outcomes (Bechara et al., 2000; O'Doherty et al., 2003). To evaluate BOLD sensitivity in the OFC, we contrasted activation during reward to that during punishment.

Design

Colored squares were presented at the center of the screen for 1500 ms. Subjects were asked to respond with a button press as quickly as possible. After 500 ms, feedback was presented for 1000 ms, and there was then an interval before the next trial randomly selected to prevent anticipation of target onset from the range 1000–2000 ms. There were three different conditions: reward, punishment, and control. Reward comprised £0.25 and a pleasant sound, and punishment the loss of £0.25 and an unpleasant sound. During the reward condition, only green squares were presented. When subjects responded faster than a set threshold, a smiley face was shown and they were rewarded. When their response was not fast enough, a sad face was shown, but there was no punishment. During the punishment condition, only red squares were presented and subjects again had to respond as quickly as possible. When their response was faster than the set threshold, a smiley face was presented, but there was no reward. When subjects responded too slowly, the sad face was shown and they were punished. Unknown to the subjects, in both conditions, the reaction time threshold for correct responses was adjusted adaptively to ensure approximately 67% of trials were rewarded in the reward condition or punished in punishment condition. The third condition was a resting baseline, with no task. During all conditions, a reward bar was presented at the side of the screen, which represented cumulative financial winnings with a maximum height worth of £5. Subjects were given £0.74 to start with and were instructed to try and win as much money as possible. In each run, six sub-blocks of each condition were presented in a pseudo-random order. Each sub-block lasted 36 s, making the total block around 11 min.

Analysis

Analysis was done using SPM 99. It was performed independently for the real and sham shims. As we were using an interleaved slice order, we first performed a slice-timing correction and then motion correction. Field-map undistortion was then applied using the methods evaluated in Cusack and Papadakis (2002) and Cusack et al. (2003). We then performed spatial normalization using cost-function masking (http://www.mrc-cbu.cam.ac.uk/Imaging/epimasking.html) and smoothing with a kernel of FWHM 10 mm. The model was a block design and comprised nine regressors, representing the three experimental conditions (reward, punishment and control) plus six movement parameters. To examine whether the shim improved functional sensitivity, a region-of-interest analysis was performed.

Results

Magnitude of field gradient (MFG) and simulated EPI image intensity (sII)

Fig. 2 shows the mean across subjects of the MFG with the sham (top panel) and real (bottom panel) shim. It can be seen by eye from this simple measure that the shim does indeed reduce the amount of field inhomogeneity. The results of the more sophisticated simulated EPI image intensity (sII) are shown in Fig. 3. The top panel shows the results with a sham shim and the middle panel the results with a real shim. A value of 100% would correspond to the intensity if there were no field inhomogeneities.

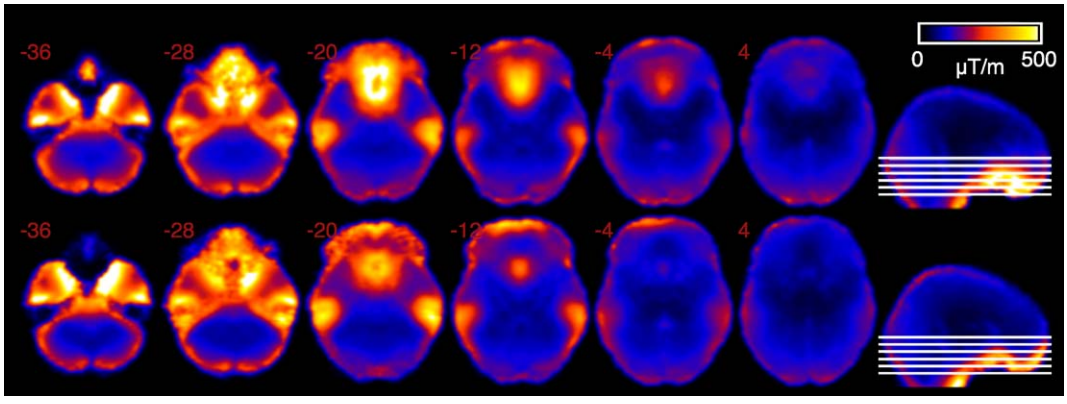

Fig. 2. Magnitude of field gradient (MFG) without and with the shim, averaged across subjects. The scale on both images is μT/m.

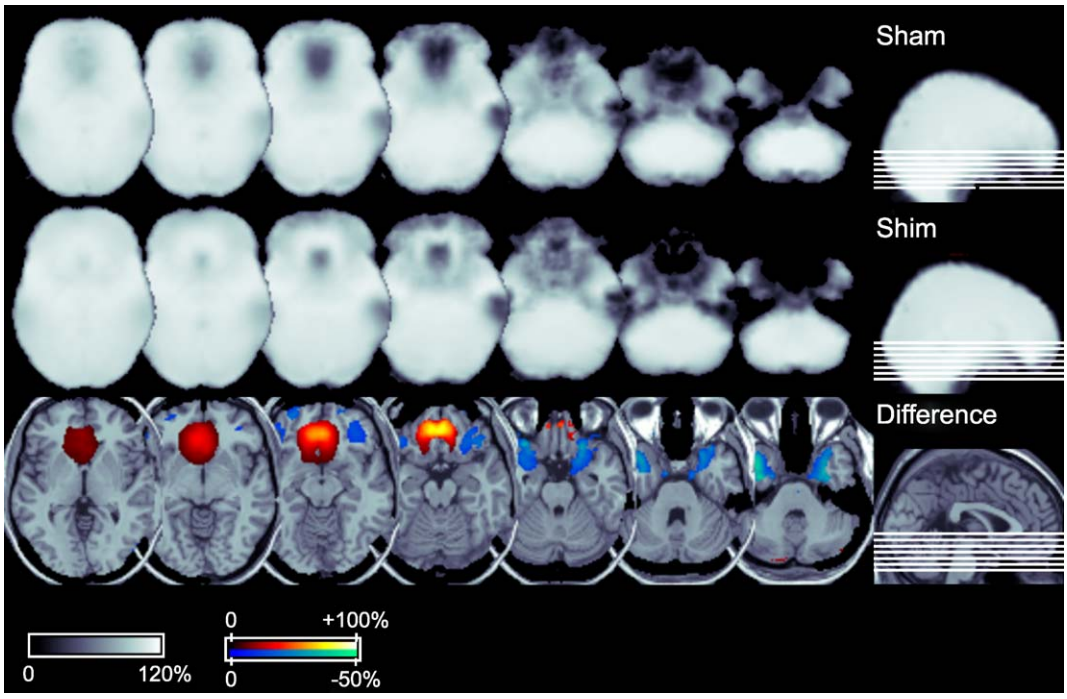

Fig. 3. Simulated EPI image intensity (sII), as estimated from the field maps using Deichmann et al's (2002) model, averaged across subjects. The top panel shows the mean estimated signal strength across subjects without the shim and the middle panel corresponding data with the shim. 100% corresponds to the amount of signal expected in the absence of field inhomogeneities. The bottom panel shows the difference between these two percentages, thresholded to only include significant values (FDR $P < 0.05$) with a difference magnitude greater than 10%.

By eye, it can be seen that the shim reduces the size of the estimated EPI signal dropout in inferior frontal cortex. To confirm that the difference was statistically significant, we performed a random effects ANOVA, comparing the 10 sII data sets with the sham shims to the 10 corresponding data sets with the real shims, using the 2-sample t test "Basic Model" in SPM99. A threshold of 0.05 using the FDR whole brain correction was then used. We found that the field map data are much less noisy than standard EPI data on which statistics are performed, and so we found that even very small differences were statistically significant. As large differences in image intensity are much more important to us than very small differences, irrespective of reliability, we selected those voxels that were not only significant at FDR = 0.05 but also where the absolute difference in sII was greater than 10% in size. The resulting maps are shown in the bottom panel of Fig. 3. There was a substantial increase in sII in frontal cortex. In a few regions in more lateral inferior frontal cortex and in the temporal lobes, there was a slight reduction in sII with the shim. However, these effects were much smaller than the positive increases (note scale differences).

Measured EPI image intensity (mII)

The measured EPI image intensity (mII) is shown in Fig. 4 with the same conventions as for Fig. 3. The top panel shows the mean EPI across subjects with the sham shim and the middle panel with the real shim. The increase in image intensity in inferior frontal cortex is clearly visible. In the bottom panel, we show the differences that are greater than ±10% which are also significant at FDR = 0.05, as for the data presented in Fig. 3. The overall pattern is similar to the simulations derived from the field maps, although the magnitudes of the changes are somewhat smaller. As with the sII maps, there are a couple of regions where there is reliable decrease in mII, in the anterior temporal lobes and in an anterior lateral inferior frontal region. This pattern of results was very consistent across subjects. To illustrate this, sample difference data for four typical individual subjects (thresholded at ±25%) are shown in Fig. 5.

Simulated BOLD sensitivity (sBS)

The second measure derived from the field maps simulates BOLD sensitivity. This is presented in Fig. 6 with the same convention as in Figs. 3 and 4. From the top panel, it is clear that the effects of field inhomogeneities on sBS are more widespread than their effect on sII (compare Figs. 3 and 6). Inspection by eye of the middle panel shows a substantial improvement when the shim is used. This was confirmed statistically, as shown in the bottom panel.

Note that there is a small but significant reduction across much of more posterior regions. A closer analysis of the field maps showed that the cause of this small effect was that the inhomogeneities in this region actually usually have a beneficial effect, in that they lengthen the echo time (i.e., $Q < 1$) to an extent that actually gives it a more optimal BOLD sensitivity. Because there is sudden dropout when effective echo time is shifted upwards above the point where the acquisition does not cover the center of k-space, the echo time on our acquisition is actually chosen to be somewhat lower than the value which would be theoretically optimum in the absence of inhomogeneities. Hence, unusually, the field inhomogeneities actually have this small beneficial effect that is abolished with better shimming.

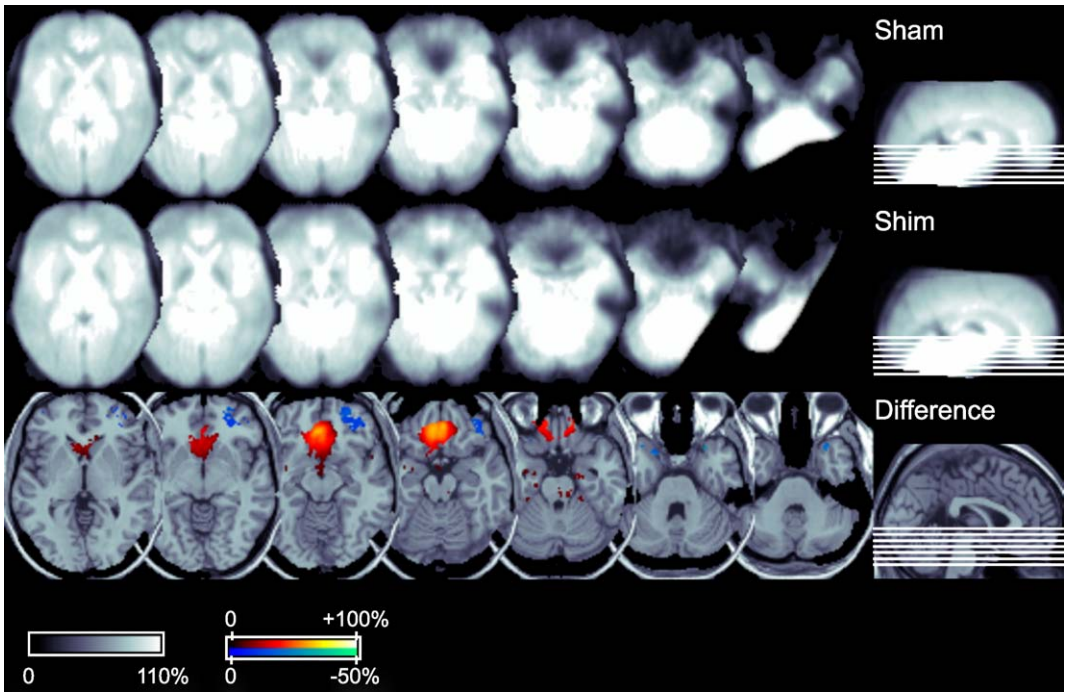

Fig. 4. Measured EPI image intensity (average mII) averaged across subjects, in the same format as used for Fig. 3.

However, this could be corrected for by increasing the echo-time a little when the shim was used.

Functional evaluation (fMRI)

Behavioral results

Data from two subjects were excluded from all analyses due to excessive movement. The behavioral data show that our manipulation of the reaction time threshold led to reward in 78% of the trials in the reward condition and punishment in 63% of the trials in the punishment condition. A difference in performance was confirmed by a 2 × 2 repeated measures ANOVA. One factor specified the type of shim (real vs. sham) and the other the condition (reward vs. punishment). The dependent measure was the proportion of trials in which the key press was fast enough. There was a main effect of condition

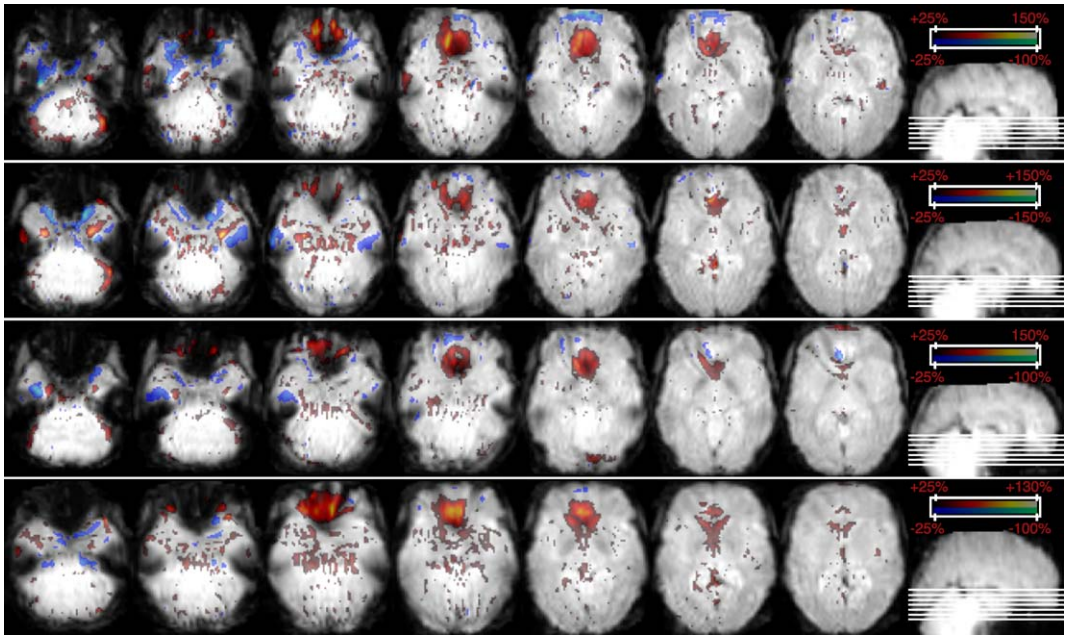

Fig. 5. Individual results for four representative passive shimming subjects—change in measured EPI image intensity with shim (individual mII) overlaid on the sham mean. The scales are as a proportion of the overall mean for each image rather than a local mean.

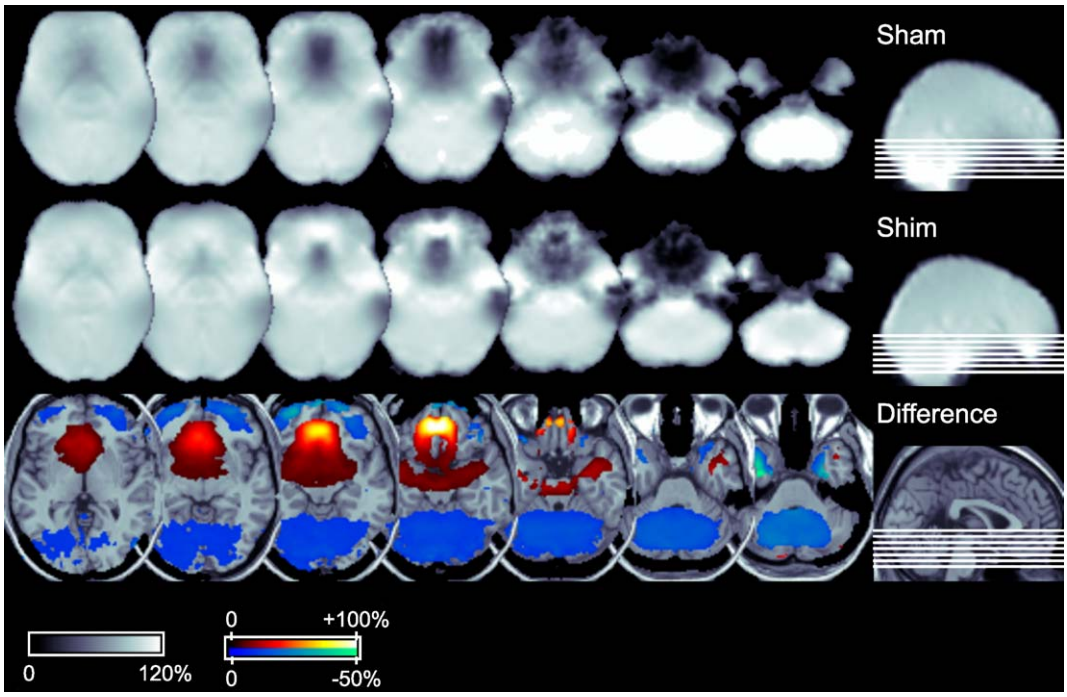

Fig. 6. Simulated BOLD sensitivity (sBS) averaged across subjects, in the same format as used for Fig. 3.

($F(1, 7) = 75.1$, $P < 0.0005$). Performance did not differ between shimming methods ($F(1, 7) = 0.664$, NS) and no interaction was found between shimming method and condition ($F(1, 7) = 2.38$, NS). Another ANOVA with the same design was performed on the actual reaction times. Subjects responded equally fast on the reward blocks as on the punishment blocks ($F(1, 7) = 0.696$, NS), and no difference was observed between the shim and sham condition ($F(1, 7) = 1.04$, NS).

Imaging results

From the contrast of the BOLD sensitivity maps between the real and sham shims, we extracted the peak, which was in orbitofronal cortex at MNI coordinates of (−6, 30, −14). A region of interest 10 mm around this was used to analyze the EPI data with the MarsBar toolbox for SPM (http://marsbar.sourceforge.net). The average across the ROI of the contrast values from a set of first level within-subject models contrasting reward to punishment were extracted, and then entered into a second level random-effects analysis. With the sham shim, no significant activation was observed ($t(7) = 0.65$), but when the real shim was used significant activation was found ($t(7) = 2.09$; $P < 0.05$). We also performed a repeated-measures ANOVA with two factors each with two levels (shim vs. sham; reward vs. punishment) which demonstrated a significant interaction of the two factors ($F(1,7) = 1.64$; $P < 0.05$), showing that there was a significantly greater difference between the reward and punishment conditions when a real shim was used.

Summary measure of regions of most improvement

There are two major advantages of using the field maps to generate a model of EPI image intensity and BOLD sensitivity. First, it helps us to confirm the origin of the cause of the improvement in image intensity. Second, it allows us to estimate the change in BOLD sensitivity that will be obtained across different brain regions. This is hard to obtain using functional activation, as each brain region would need to be activated using a different functional task.

We used our simulated BOLD sensitivity maps to provide a summary measure of where the BOLD signal should be improved most, using the AAL map to provide a set of regions-of-interest. In each region, the mean improvement was quantified. The results are shown for all 116 regions of the AAL map in Fig. 7, and for the 12 regions where there was the most reliable improvement as measured using a t statistic in Fig. 8. Appendix 1 lists the AAL regions in the same order as they are shown in Fig. 7.

Discussion

We have shown that the use of a passive shim improves field homogeneity (reduces MFG) in orbitofrontal cortex and anterior midbrain regions. In these areas, it increases simulated and measured EPI image intensity (sII, mII) substantially. Over a wider region there was also an increase simulated BOLD sensitivity (sBS). Finally, we showed using a reward–punishment task that the use of a passive shim improves measured functional activation (fMRI). We did find some small costs of the shim: slightly reduced simulated and measured EPI image intensity (sII, mII) in anterior and lateral inferior frontal cortex, and in the anterior inferior temporal lobes. There was a small decrease in simulated BOLD (sBS) sensitivity over much of the brain away from inferior frontal regions.

Our results replicate those of Wilson et al. (2002) and extend them in several important ways. Whereas they only examined

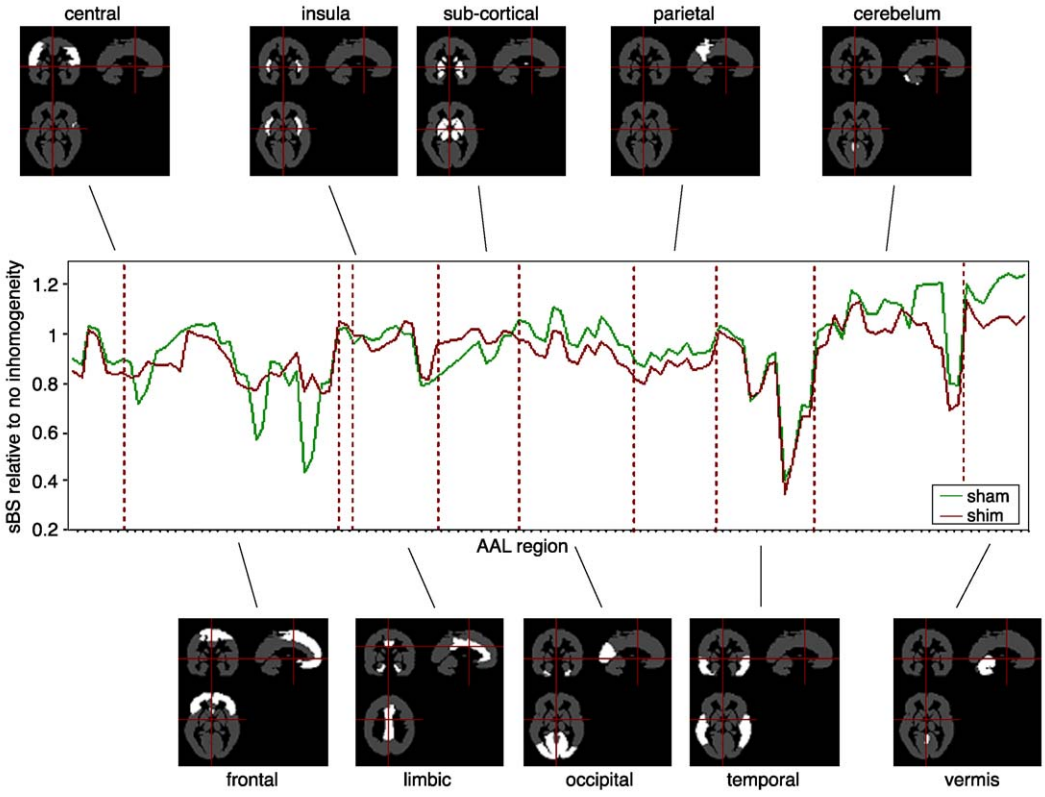

Fig. 7. Simulated BOLD sensitivity (sBS) averaged across subjects partitioned by AAL region. The AAL regions are listed in Appendix 1, in the order in which they are arranged along the *x*-axis.

signal changes in inferior frontal regions, we have performed whole-brain analyses to show where in the brain signal is affected by the shim. We have used a sophisticated model of the effect of field inhomogeneity on EPI sequences. The first part of this model provides a simulation of EPI image intensity that predicts well what was actually obtained. The second part simulates the BOLD sensitivity, which is what is actually most important in the design of experiments. We have generated summary measures using the AAL map to describe where the improvements are. And, for the first time, we have conducted an empirical assessment of functional sensitivity, using a reward–punishment task.

Several other methods exist for improving sensitivity in the inferior frontal and anterior temporal regions. One is to use Positron Emission Tomography rather than fMRI. This may indeed be the best solution in some circumstances, but the benefits of MRI are many. For example, there is no need to administer a radioactive dose, and so a larger selection of the population may be scanned, and repeated sessions may be performed. Spatial resolution and power are generally higher. Another option is to attempt to optimize imaging parameters such as the slice angle and thickness. This has been done by Chen et al. (2003) for the amygdala, and Gustard et al. (2001) for the motor cortex. As the field gradients themselves are rapidly changing in direction in inferior frontal regions; however, it is likely that is only ever possible to optimize small regions in this way. This approach was extended by Deichmann et al. (2003) who combined slice angle optimization with corrective preparation pulses.

Yet another option for improving signal in regions with dropout is to apply corrective gradients (e.g., Deichmann et al., 2002). This holds good potential, but again it will only be practically possible to optimize signal across a limited region, and the additional acquisitions required increase the TR and reduce the sensitivity per unit time in other regions. An exciting possibility is to combine the passive shimming and corrective gradient techniques. It might be that passive shimming reduces

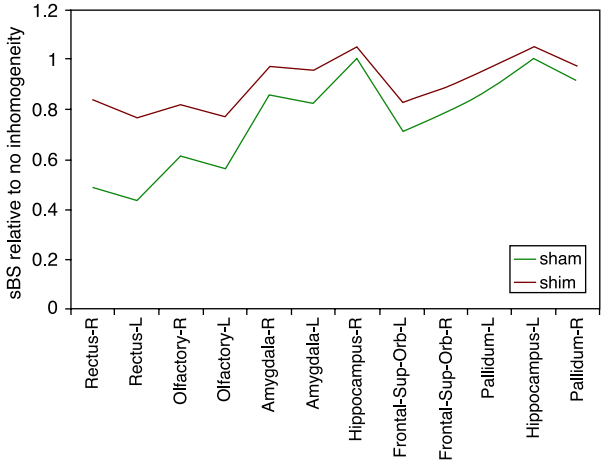

Fig. 8. The 12 AAL regions showing the most reliable simulated BOLD sensitivity (sBS) improvement.

the gradients over a wider region to a level where they can be corrected by corrective gradients.

As in the study by Wilson et al. (2002), we used a single shim for all subjects rather than customizing the shim shape for each person. It is encouraging that a single default shim can lead to substantial improvements, as this simplifies the procedure substantially. However, it might be useful to evaluate in the ways we have presented the additional improvement obtained by customizing the shims to the participants, such as in the work of Wilson et al. (2003).

The use of fMRI in addition to the generation of BOLD sensitivity maps is important because there are several effects that are not considered in the sensitivity maps. For example, the effects of subject movement are not modeled. The demonstration of an improvement in functional sensitivity in the presence of a shim, even when there will have inevitably been some subject motion, is in agreement with the simulations and data presented by Wilson and Jezzard (2003). They showed increased signal stability in the presence of movement when a shim was used. Another aspect not modeled in the BOLD sensitivity model is that some of the noise in the signal will not come from machine sources (e.g., thermal noise) but physiological ones (e.g., blood pulsation). Reduced image intensity scale this noise by the same factor as the signal, and so according to this argument, just because signal level is reduced, signal-to-noise may not be. Against this last argument, however, is the common experience of difficulty in activating inferior frontal cortex, and our demonstration of a functional improvement with shimming shows that power to detect activation is affected by field inhomogeneities.

We scanned our subjects on four blocks totaling 44 min, and none of our participants reported finding the shim excessively uncomfortable, although one did report that it dried the mouth and was a little unpleasant. The plastic mouth molds for the shims are reasonably simple to make, taking 10–15 min with each subject. Construction could easily be done just before scanning takes place, although two blocks would be useful if subjects are to be placed in the scanner consecutively.

In summary, passive shims generally increase field homogeneity, simulated and measured EPI image intensity, and simulated and measured BOLD sensitivity. They are quick to make, and were found to be fairly comfortable. The procedure could be of great use to many researchers studying inferior frontal and anterior temporal regions.

Acknowledgments

We would like to thank Dr. Kalina Christoff, who helped with the design of the functional task, and Dr Chris Rorden whose list of the AAL regions we used (provided with www.mricro.com). We would also like to thank the MRC (UK) for funding the project.

Appendix A. AAL regions used in Fig. 7 (from www.mricro.com)

1	Precentral_L	31	Cingulum_Ant_L	61	Parietal_Inf_L	91	Cerebelum_Crus1_L
2	Precentral_R	32	Cingulum_Ant_R	62	Parietal_Inf_R	92	Cerebelum_Crus1_R
3	Frontal_Sup_L	33	Cingulum_Mid_L	63	SupraMarginal_L	93	Cerebelum_Crus2_L
4	Frontal_Sup_R	34	Cingulum_Mid_R	64	SupraMarginal_R	94	Cerebelum_Crus2_R
5	Frontal_Sup_Orb_L	35	Cingulum_Post_L	65	Angular_L	95	Cerebelum_3_L
6	Frontal_Sup_Orb_R	36	Cingulum_Post_R	66	Angular_R	96	Cerebelum_3_R
7	Frontal_Mid_L	37	Hippocampus_L	67	Precuneus_L	97	Cerebelum_4_5_L
8	Frontal_Mid_R	38	Hippocampus_R	68	Precuneus_R	98	Cerebelum_4_5_R
9	Frontal_Mid_Orb_L	39	ParaHippocampal_L	69	Paracentral_Lobule_L	99	Cerebelum_6_L
10	Frontal_Mid_Orb_R	40	ParaHippocampal_R	70	Paracentral_Lobule_R	100	Cerebelum_6_R
11	Frontal_Inf_Oper_L	41	Amygdala_L	71	Caudate_L	101	Cerebelum_7b_L
12	Frontal_Inf_Oper_R	42	Amygdala_R	72	Caudate_R	102	Cerebelum_7b_R
13	Frontal_Inf_Tri_L	43	Calcarine_L	73	Putamen_L	103	Cerebelum_8_L
14	Frontal_Inf_Tri_R	44	Calcarine_R	74	Putamen_R	104	Cerebelum_8_R
15	Frontal_Inf_Orb_L	45	Cuneus_L	75	Pallidum_L	105	Cerebelum_9_L
16	Frontal_Inf_Orb_R	46	Cuneus_R	76	Pallidum_R	106	Cerebelum_9_R
17	Rolandic_Oper_L	47	Lingual_L	77	Thalamus_L	107	Cerebelum_10_L
18	Rolandic_Oper_R	48	Lingual_R	78	Thalamus_R	108	Cerebelum_10_R
19	Supp_Motor_Area_L	49	Occipital_Sup_L	79	Heschl_L	109	Vermis_1_2
20	Supp_Motor_Area_R	50	Occipital_Sup_R	80	Heschl_R	110	Vermis_3
21	Olfactory_L	51	Occipital_Mid_L	81	Temporal_Sup_L	111	Vermis_4_5
22	Olfactory_R	52	Occipital_Mid_R	82	Temporal_Sup_R	112	Vermis_6
23	Frontal_Sup_Medial_L	53	Occipital_Inf_L	83	Temporal_Pole_Sup_L	113	Vermis_7
24	Frontal_Sup_Medial_R	54	Occipital_Inf_R	84	Temporal_Pole_Sup_R	114	Vermis_8
25	Frontal_Mid_Orb_L	55	Fusiform_L	85	Temporal_Mid_L	115	Vermis_9
26	Frontal_Mid_Orb_R	56	Fusiform_R	86	Temporal_Mid_R	116	Vermis_10
27	Rectus_L	57	Postcentral_L	87	Temporal_Pole_Mid_L		
28	Rectus_R	58	Postcentral_R	88	Temporal_Pole_Mid_R		
29	Insula_L	59	Parietal_Sup_L	89	Temporal_Inf_L		
30	Insula_R	60	Parietal_Sup_R	90	Temporal_Inf_R		

References

Bechara, A., Damasio, H., Damasio, A.R., 2000. Emotion, decision making and the orbitofrontal cortex. Cereb. Cortex 10 (3), 295–307.

Chen, N.K., Dickey, C.C., Yoo, S.S., Guttmann, C.R., Panych, L.P., 2003. Selection of voxel size and slice orientation for fMRI in the presence of susceptibility field gradients: application to imaging of the amygdala. NeuroImage 19, 817–825.

Cusack, R., Papadakis, N., 2002. New robust 3-D phase unwrapping algorithms: application to magnetic field mapping and undistorting echoplanar images. NeuroImage 16, 754–764.

Cusack, R., Brett, M., Osswald, K., 2003. An evaluation of the use of magnetic field maps to undistort echo-planar images. NeuroImage 18, 127–142.

Deichmann, R., Josephs, O., Hutton, C., Corfield, D.R., Turner, R., 2002. Compensation of susceptibility-induced BOLD sensitivity losses in echo-planar fMRI imaging. NeuroImage 15, 120–135.

Deichmann, R., Gottfried, J.A., Hutton, C., Turner, R., 2003. Optimized EPI for fMRI studies of the orbitofrontal cortex. NeuroImage 19, 430–441.

Elliott, R., Newman, J.L., Longe, O.A., Deakin, J.F., 2003. Differential response patterns in the striatum and orbitofrontal cortex to financial reward in humans: a parametric functional magnetic resonance imaging study. J. Neurosci. 23 (1), 303–307.

Genovese, C.R., Lazar, N.A., Nichols, T., 2002. Thresholding of statistical maps in functional neuroimaging using the false discovery rate. NeuroImage 15, 870–878.

Gottfried, J.A., Deichmann, R., Winston, J.S., Dolan, R.J., 2002. Functional heterogeneity in human olfactory cortex: an event-related functional magnetic resonance imaging study. J. Neurosci. 22 (24), 10819–10828.

Gustard, S., Fadili, J., Williams, E.J., Hall, L.D., Carpenter, T.A., Brett, M., Bullmore, E.T., 2001. Effect of slice orientation on reproducibility of fMRI motor activation at 3 Tesla. Magn. Reson. Imaging 19, 1323–1331.

Knutson, B., Fong, G.W., Adams, C.M., Varner, J.L., Hommer, D., 2001. Dissociation of reward anticipation and outcome with event-related fMRI. NeuroReport 12 (17), 3683–3687.

O'Doherty, J., Kringelbach, M.L., Rolls, E.T., Hornak, J., Andrews, C., 2001. Abstract reward and punishment representations in the human orbitofrontal cortex. Nat. Neurosci. 4 (1), 95–102.

O'Doherty, J.P., Deichmann, R., Critchley, H.D., Dolan, R.J., 2002. Neural responses during anticipation of a primary taste reward. Neuron 33, 815–826.

O'Doherty, J., Critchley, H., Deichmann, R., Dolan, R.J., 2003. Dissociating valence of outcome from behavioral control in human orbital and ventral prefrontal cortices. J. Neurosci. 23 (21), 7931–7939.

Small, D.M., Zatorre, R.J., Dagher, A., Evans, A.C., Jones-Gotman, M., 2001. Changes in brain activity related to eating chocolate: from pleasure to aversion. Brain 124 (Pt. 9), 1720–1733.

Tzourio-Mazoyer, N., Landeau, B., Papathanassiou, D., Crivello, F., Etard, O., Delcroix, N., Mazoyer, B., Joliot, M., 2002. Automated anatomical labeling of activations in SPM using a macroscopic anatomical parcellation of the MNI MRI single-subject brain. NeuroImage 15, 273–289.

Wilson, J.L., Jezzard, P., 2003. Utilization of an intra-oral diamagnetic passive shim in function MRI of the inferior frontal cortex. Magn. Reson. Med. 50, 1089–1094.

Wilson, J.L., Jenkinson, M., Jezzard, P., 2002. Optimization of static field homogeneity in human brain using diamagnetic passive shims. Magn. Reson. Med. 48, 906–914.

Wilson, J.L., Jenkinson, M., Jezzard, P., 2003. Protocol to determine the optimal intraoral passive shim for minimisation of susceptibility artifact in human inferior frontal cortex. NeuroImage 19, 1802–1811.